Morphology of Surface Integrity as Effect of Cold Forging of Aluminum Alloy

Catalin Pruncu, Tat Thang Pham, André Dubois, Mirentxu Dubar, Laurent Dubar

Morphology of surface integrity as effect of cold forging of aluminum alloy

Catalin I. Pruncu[1]*, T T Pham[2], A. Dubois[2], M. Dubar[2], L. Dubar[2]

[1] Mechanical Engineering, University of Birmingham, Edgbaston, B15 2TT, United Kingdom
[2] University of Valenciennes and Hainaut Cambresis, LAMIH UMR 8201, F-59313, Valenciennes, France
* Corresponding author. Tel: c.i.pruncu@bham.ac.uk.

Abstract

Aluminum and its alloys represent a common raw material for components released through a cold machining routine (i.e. forging, cold heading and rolling process). They offer easy manufacturing and high performance of plastic strength, together with light weight, long lifespan and easy recycling; and are heavily used in the transport industry [1] [2]. However, during processing the sample/tool interfaces can generate sticking mechanisms that produce growth in the friction values and high wear rate, leading to irreversible damage of the workpiece surface. The surface morphology provides characteristics that allow detection of the damage amplitude. The hard contact between asperities causes nucleation and formation of adhesive wear. The normal load and lubrication conditions may further affect the quantity of wear elements [3]. Optical non-destructive observations permit the detection of the quantity of wear elements as per material transfer from one side (specimen surface) to the other side (contactor surface).

This paper presents the mechanisms of the adhesive layer, of material transfer, that are directly proportional to the new roughness stature. A robust Finite Element Method (FEM) analysis was embedded to establish a relationship between time, the plastic deformations, friction coefficients and surface defects.

Keywords: aluminum alloy; cold forging; wear characteristics; FEM

1. Introduction

Lightweight and robust structures have proven useful for innovative applications within the automotive industry [4]. A good surface finish during the manufacturing routine represents an important parameter that sustains the emergent trend of lightweight structures. Aluminum and its alloys may fit within these requirements, being an efficient solution in terms of processing and cost. Most studies reveal the great achievement of aluminum alloys, by using cold manufacturing (cold forging, cold heading and cold rolling process), as a principal raw material.

However, the contact conditions between tool and workpiece are vital in optimization of such processes. Tribological tests have been developed to better understand this complex phenomenon of friction and wear mechanisms during metal forming processes: for example, the ring compression tests, alternative ring-compression tests, pin-on-disc configuration, a modified cylinder-on-cylinder test with a spring loading system, and/or a new load-scanning test method, among others [5], [6], [7], [8], [9]. The contact pressure is a common parameter that affects the friction coefficients while substantial interface contact behavior occurs [10]. Friction stress at tool/workpiece interfaces depends on the local peaks of temperature that gradually increase as the sliding velocity rises and may be further accentuated by the increase of billet radius causing higher dissipation of friction energy [11] and of course of tool radii [12].The positioning of the surface and the reduction in sample height, at the contact interface, during the upsetting procedure also lead to an increase in the values of friction coefficients [13]. Boric acid films which can be firmly adhered to clean aluminum surfaces by spraying their methanol solutions may provide extremely low friction coefficients (~0.04); thus, preventing direct contact and preserving the surface qualities [14].

Heinrichs et al. [15], [16] applying multi-stage sliding tests, detected a gradual increase in the value of friction forces due to progressive sticking. It was found that the friction coefficient is directly related to the amount of workpiece material transferred to the tool which in turn depends on the microstructure of the tool steel. It appears that the coefficient of friction (COF) can increase with each pass, until it reaches saturation level. This progression is accompanied by a gradual increase in the number of transferred layers of material, which lead to roughening of the tool surface [17].

Kirkhorn et al. [18] reproduced the forming routine by a tribo-tester based on a flat-die strip drawing. Considering the contact area, normal pressure, sliding speed, lubricant and surface characteristics, they found that tribological behavior depends mainly on tool microstructure and the contact pressure is governed by lubrication conditions. [9] confirmed this concept by performing compression drawing tests in order to obtain the formation of bosses. They found that it is possible to acquire the prominent form of "bosses" with moderate punch pressure using only one side of the blank lubricated.

This report presents details concerning the adhesive layer of material transfer and its mechanism produced during the forming process. It is observed that the amount of surface covered by the material transfer depends on plastic deformation. The embedding of the numerical simulations allows further improvement of sticking mechanisms. A relationship between plastic deformations, friction coefficients and surface defect deposition was recognized.

2. Material characteristics

Samples made of aluminum alloy Al6082 with 2.0 mm thickness were considered in this research. Aluminum alloy 6082 is a medium strength alloy with good weldability, brazeability, corrosion resistance, formability and machinability. This grade is used in substitution to the conventional 6061 alloys in many structural applications in which improved mechanical properties are required [19]. Rods, bars and machining stocks, seamless aluminum tubing, structural profiles and custom profiles are widely used in transport and structural applications in which high stress resistance is essential [20]. Mechanical properties of the Al6082 T6 studied are as follow: the Yield stress, Re ~280 (MPa); the Ultimate strength, Rm ~333 (MPa); the Young's modulus, E ~69 (GPa) and the Elongation at fracture, A ~12%. The chemical compositions of this material include Mg~0.60, Si~0.7, Fe~0.24, Cu~0.06, Mn~0.9, Cr~0.02, Zn~0.06, Ti~0.02.

The mechanical behavior of the Al6082 material was assessed via a quasi-static tension test, with a crosshead speed displacement of 0.5 mm/s. During the testing process, tensile strain developed in specimens was measured with an extensometer. The average stress-strain (σ–ε) curves derived from six experimental tests are plotted in Figure 1.

3. Parameters and set up

The nominal dimensions of the 46 specimens tested in this study are as follows: L=40 mm, l=10 mm, and h=2 mm, surrounded in Fig. 2. The geometry of the contactors was reproduced from [21]; except for the contour radius that is 20 mm. Upsetting sliding tests were performed with respect to the following conditions:

- penetration depth (contactor within the specimen), Δh: 0.04, 0.07, 0.095, 0.12, 0.18 mm;
- sliding velocity, V_S: 10mm/s (for 22 samples tested), 60mm/s (for 22 samples tested);
- True sliding distance: 40 mm;
- Specimen and contactor temperatures: room temperature (≈ 20°C)
- Mean arithmetic surface roughness of the contactors: Ra ≈ 0.3 μm;
- Lubricant: dry test and lubricated MoS_2 (thickness of solid lubricant layer about 10 μm);

Each test was performed with a new contactor.

The initial roughness of the contactor and of the specimen is shown in Figure 3. Both surfaces are orthotropic. USTs are performed so that the sliding direction corresponds to the longitudinal direction "L" of the specimens. It can be noticed that all surfaces have a uniform level of roughness asperities in any region of the inspected surfaces.

The surface of the specimen may become scratched during the UST. This involves damage accumulation on both specimen and contactor surfaces. The rate of surface degradation may be expressed as a function of penetration depth due to possible transfer of material from specimen to the contactor; more localised and severe degradation of the contactor surface will occur as a result of increasing penetration depth.

Very early damage of the sample surface may be avoided and the steady state friction phase can be detected performing tests when the specimens are lubricated (i.e. by molybdenum disulphide (MoS2) solid lubricant). This medium may reduce the direct contact between contactor and workpiece sample, and finally lead to a significant decrease of wear damage.

3.1. Numerical modelling

To obtain a better understanding of the plastic deformation activity produced at the tool/workpiece interface while forming was replicated, a finite element model analysis was created for each experimental test. Experimental results were used as boundary conditions for numerical simulations.

2D solid body models were modelled for the samples subjected to plane strain with nominal dimensions, as detailed in Section 3. The fixed stand and the contactor were modelled as rigid elements. The "model" was discretized into implicit CPE4R elements, having the element size of 0.1 mm determined via convergence analysis. In the numerical computation, the coefficient of friction was inserted from the experimental UST results according to [21].

A mathematical power curve $\sigma=K\times\varepsilon n$ MPa as indicated in the E646 ASTM International Standard [22] was embedded to detect the parameters of the stress-strain curve, and later inserted in ABAQUS 6.12. Thus, the material strength coefficient K=498 and hardening exponent n=0.101 were used.

3.2. Statistical setup of plastic deformation

The statistical determination was verified by taking into account 22 (i.e. forming tests, due to the same range of plastic strain shown for both simulations; 10 and 60mm/s) trial experiments performed under the USTs. Plastic strain achieved in the vicinity of the contact zone ranged from 0.006 to 0.112. Sturges' rule was used to define "classes" of plastic strain [23] delimiting the large range of values. The classes were delimitated for a limited number as:

$$k=1+3.332*\text{Log}(N), \text{ where } N=22 \text{ (tests)} \quad (1)$$

The range of plastic deformation Ep for different values was associated to an imposed penetration depth.

$$Ep=\varepsilon_{max}-\varepsilon_{min} \quad (2)$$

Where: ε_{max} of 0.112 (i.e. a maximum of plastic deformation generated at the interface between contactor/specimen using a penetration depth $\Delta h=180\mu m$); ε_{min} of 0.006 (i.e. a maximum plastic

deformation generated at the interface between contactor/specimen using a penetration depth of $\Delta h=40\mu m$).

The length of each grade is obtained from the relationship:

$$L=Ep / k \quad (3)$$

The allocated classes, corresponding to upper and lower limits defined on the basis of Eqns. (1-3), that make possible the determination of the mean values and corresponding standard deviations are summarized in Table 1.

4. Assessment of surface integrity

4.1. Quantification of material transfer onto the contactor

The thickness of a local layer of material transferred on the tool was evaluated by inspecting the tool surface before and after the forming sequence. For this purpose, the maximum ten-point height (Rz) was determined using Eq. (4). In this measurement, the difference between the averages of the 5 highest and 5 lowest points on the surface was computed. Figure 4 shows a standard measure chain for a typical specimen investigated in this research.

$$Rz = \frac{(P1+P2...+P5)-(V1+V2...+V5)}{5} \quad (4)$$

The difference between the final and initial form of the profile thickness corresponds to the thickness of the layer, of aluminum material, transferred from the specimen to the contactor. Figure 5 provides details of the amount of material transferred onto the contactor surface as a function of the range of plastic strain. It appears that the thickness of the transfer layer increases with plastic deformation. The amount of material deposited onto the tool surface may not be significant at low plastic strain, as in the deformation grades Ep1 to Ep4 (see Figure 5). Also, it seems that the transferred material spreads homogenously on the tool surface and does not depend on sliding direction.

Correlation between optical profilometry and SEM observations is of fundamental importance because it may provide fundamental insight regarding the UST procedures and allow the

detection of when breaking of the lubricant film occurs. In particular, 3D-Optical profilomety may help in detecting the real thickness of the surface defect deposited on the tool surface. On the other hand, the SEM observations provide topographical and morphological details on the surface defect deposition. Details of major observations are introduced in Figure 6.

Figure 6 shows the 3D-profilomety and SEM patterns recorded for the contactor surface at different levels of plastic strain. The SEM topography of sliding tracks reveals some typical rolling marks achieved on the rolled aluminum surfaces, appearing as narrow and deep wear scars extended along the sliding direction. The aluminum rolled surfaces may generate as a strong presence of aluminum-iron oxides that could be a consequence of the mechanical mix of the removed and transferred material during the mechanical routine [24]. It can be seen that the amount of material transferred from the workpiece to the contactor increases with plastic deformation and almost covers the whole surface of the tool for the very large plastic deformation of grade Ep5 (see Figure 5 (g). The same behavior (i.e. massive materials transfer) was observed in case of dry forging (i.e. without lubricant), as shown in Figure 6 (h). Obviously, even for a small plastic deformation (Ep1) the SEM patterns starts to emphasize the wear adhesion as the primary type of defect encountered on the tool surface, in good agreement with [15] studies that have indicated the aluminum adherence on the tool surface starts on the first contact. The transfer mechanism may develop through adhesion of aluminum to steel and delamination of aluminum particles which are subsequently smeared on the aluminum surface. The initial interactions between aluminum and iron at asperity level and, with progressive transfer, it changes to that of aluminum and aluminum. This was very well reflected, in Figure 6, in the iron content present on the worn surface as found by SEM analysis. The edges of the plastically deformed material is cracking up leading of the detachment of a debris [25]. In this process, the wear particles are transferred away from the center of the contact area leaving the underlying metal exposed. In case of smooth wear, the surface is enriched in Si but when galling occurs the silicon is strapped aside and the hard silicon surface is probably responsible to some degree for the damage, as well as iron transfer to the aluminum surface [26].

4.2. Evolution of friction

Figure 7 plots the values of coefficient of friction with respect to the level of plastic strain developed in zone II. An average friction coefficient value corresponding to a standard deviation evaluated for each level of plastic strain was computed. The MoS_2 lubricant used in the UST routine helps to reduce the value of the coefficient of friction from 0.5-0.7 (values determined from the two non-lubricated USTs.) to 0.06-0.15.

It is obvious, that the Coulomb friction coefficient has a low value as long as the plastic strain remains in the Ep1 to Ep4 grade range for an initial speed of 10mm/s, and is related to the thickness value of material transfer (max. 5 μm) [27]. This process may occur due to material transfer that is fully immersed in the MoS_2 "layer" (since the thickness of the lubricant is 10μm) applied before initiating the UST process. The results are consistent with the findings of Masters et al. [28] who measured a uniform value of coefficient of friction in strip draw tests on aluminum alloys for strain levels up to 0.10. Although solid wax lubricants were utilised in the studies by Masters et al. [28], the results gathered in the present study prove good correspondence. As expected, the coefficient of friction strongly increases as deformation grade evolves from Ep4 to Ep5, as a consequence of the major level of thickness of material transfer measured for domain Ep5 (practically 20 μm).

Moreover, insignificant fluctuations in coefficient of friction values may derive from having imposed different process parameters, small variations of temperature, roughness discrepancies, or solid lubricant inhomogeneity. However, differences in coefficient of friction values were not found to be statistically significant.

When the processing speed is changed to 60mm/s, the plastic strain within the range Ep1 to Ep3 produces a gradual exponential growth of COFs followed by stabilization. The Ep5 plastic strain section reveals a new slight intensification of COF rate. A major statistical variation was achieved described by the large area of material transfer. Galling damage occurs when the lubricant fails to separate the two surfaces and adherence followed by the transfer of aluminum onto the steel surface takes place. In this case, aluminum wear and galling occurs via a process involving crack formation and propagation and delamination of particles from the metal surface.

The presence of a lubricant or anti-wear films prevent the hard contact metal-to-metal contact and damage of the aluminum surface [26].

4.3. The workpiece surface characteristics

The process of damage occurring on the tool surface may strongly affect the surface integrity of the workpiece surface. As long as the degradation of tool surface occurs, and the thickness of material deposition grows (as a proportion of plastic strain) on the top of the tool surface, the machined surface appears to become more and more degraded, showing visible craters and cracks. A consistent relationship between tool damage and workpiece integrity has been established, as emphasized in Figure 8.

The results acquired by 3D-optical profilometry, in Figure 8 a), show a map with the evolution of workpiece surface while the plastic strain increases. It seems that at low plastic strain (Ep1-Ep2) the macroscopic modification on the workpiece surface produces an isotropic structure that presents the same stature in all directions, especially for low speed. However, when the stain increases to Ep5 the orthotropic modification on the workpiece surface appears, as tool degradation evolves while increasing the material transfer, as per Ep3 to Ep5. The change in the machining speed may accelerate further the progress of surface degradation, as can be observed in Figure 8b) in respect to Figure 8c). The SEM observations permit a better interpretation of the structure morphology achieved by profilometry measurements. When the imposed penetration develops a range of plastic deformation that covers the Ep1-Ep2 interval, the workpiece surface processed presents homogenous morphology with a low value of roughness. However, the rough pitch rises in the Ep3 interval (see Figure 8a, b, and c for Ep3). The workpiece surface behaves almost orthotropically with a significant number of peaks and shallow valleys in the Ep4-Ep5 interval. The numerical simulation (in Figure 8d) provides insight as to how plastic deformation acts inside of the workpiece structure that is of vital importance to understand the evolution of surface integrity. The numerical model reveals that at low plastic strain, from Ep1 to Ep2 interval, a homogeneous material behavior occurs over the entire workpiece depth that means this loading produces only superficial modification of the workpiece surface. However, when the loading increases, the stresses tend to accentuate near the interface when the value of Ep reaches

the grade Ep5; the contact generates large deformation at the interface between tool and workpiece and the sticking mechanism is very unpredictable, creating an orthotropic surface. Corroborating the numerical simulation with the profilometry measures and SEM observations permits the validation of the numerical tool as a design solution to predict the surface integrity of the workpiece and thus predict with accuracy when the tool needs replacement.

Conclusion

This research highlights the relationships between equivalent plastic deformations developed in a workpiece during cold forming, friction coefficients, and material transfer caused by the hard surface interactions. A formal-numerical method was validated as a design solution to predict the surface integrity of the workpiece and thus predict with accuracy when the tool needs replacement. The experimental and numerical approaches used in this work prove that in the presence of lubrication (MoS2), the thickness of the aluminum transfer onto the tool surface may have very low effects on the workpiece surface integrity for a plastic strain in the range Ep1-Ep4; the average thickness of the aluminum layer transferred onto the tool surface is between 1.5 and 19.5 μm; the coefficients of friction measured during the cold forming tests present a low value while the size of aluminum deposited onto the tool surface belongs to grade Ep4, especially for low speeds up to 10mm/s. In that case, the thickness of material deposition on the tool surface may be approximately 5μm; friction coefficients show a critical value when the plastic deformation reaches the Ep5 interval and the tool surface presents a critical surface defect. This process may lead to significant wear surface events for both counterparts (tool/workpiece). The progress of wear on the tool surface can be attributed to the adhesion mechanism.

To further improve the understanding of the cold forming processes and to optimize the results may require the introduction of an extended approach focused on different geometrical and physical parameters (for reference; changing the tool shape/material, by using different types of lubricants (solid or liquid), processing temperature (from 23° to possibly 100°), multi-pass strategy, etc).

Acknowledgements

The present research work has been supported by International Campus on Safety and Intermodality in Transportation, the Nord-Pas-de-Calais Region, the European Community, the Regional Delegation for Research and Technology, the Ministry of Higher Education and Research, and the National Center for Scientific Research. The authors gratefully acknowledge the support of these institutions

References

1. Moreira, P.M.G.P., de Jesus, A.M.P., Ribeiro, A.S., P.M.S.T. de Castro,. 2008, Fatigue crack growth in friction stir welds of 6082-T6 and 6061-T6 aluminium alloys: A comparison. Theoretical and Applied Fracture Mechanics 50, 81–91.

2. Yoshimura, H., Tanaka, K.,. 2000, Precision forging of aluminum and steel. Journal of Materials Processing Technology 98, 196-204.

3. Alan Hase, Hiroshi Mishina. Wear elements generated in the elementary process of wear. Tribology International, 42 (2009) 1684–1690, Tribology International, Volume 42, Issues 11–12, December 2009, Pages 1684–1690.

4. Farrahi, G.H., Ghodrati, M., Azadi, M., Rezvani Rad, M. *Stress–strain time-dependent behavior of A356.0 aluminum alloy subjected to cyclic thermal and mechanical loadings. .* Mech Time-Depend Mater 18, 475–491 (2014) .

5. Noh, J.H., Min, K.H., Hwang, B.B.,. 2011, Deformation characteristics at contact interface in ring compression. Tribology International 44, 947–955.

6. Robinson, T., Ou, H., Armstrong, C.G.,. 2004, Study on ring compression test using physical modelling. Journal of Materials Processing Technology 153–154, 54–59.

7. Tan, X., Martins, P.A.F., Baya, N., Zhang, W.,. 1998, Friction studies at different normal pressures with alternative ring-compression tests. Journal of Materials Processing Technology 80-81, 292-297.

8. Podgornik, B., Hogmark, S., Pezdirnik, J.,. 2004, Comparison between different test methods for evaluation of galling properties of surface engineered tool surfaces. Wear 257, 843–851.

9. Wang, Z.G., Yoshikawa, Y., Osakada, K.,. 2013, A new forming method of solid bosses on a cup made by deep drawing. CIRP Annals - Manufacturing Technology 62, 291–294.

10. Hua-Chu Shih and William R. D. Wilson. 1999, Effects of Contact Pressure and Strain on Friction in Sheet-Metal Forming. Tribology Transactions Vol. 42 , Iss. 1.

11. Bay, N., Eriksen, M., Tan, X., Wibom, O.,. 2011, A friction model for cold forging of aluminum, steel and stainless steel provided with conversion coating and solid film lubricant. CIRP Annals - Manufacturing Technology 60, 303–306.

12. L. R. Sanchez. 1999, Experimental Investigation of Friction Effects Enhanced by Tool Geometry and Forming Method on Plane Strain Sheet Metal Forming. Tribology Transactions Vol. 42 , Iss. 2.

13. Azushimaa, A., Yoneyama, S., Utsunomiya, H.,. 2012, Coefficient of friction at interface of lubricated upsetting process. Wear 286– 287, 3– 7.

14. Jianjun Wei, Ali Erdemir, and George R. Fenske. 2000, Dry Lubricant Films for Aluminum Forming. Tribology Transactions Vol. 43 , Iss. 3,.

15. Heinrichs, J., Olsson, M., Jacobson, S.,. 2013, Influence of tool steel microstructure on initial material transfer in metal forming – In situ studies in the SEM. Wear 302, 1249–1256.

16. Heinrichs, J., Olsson, M., Jacobson, S.,. 2012, Mechanisms of material transfer studied in situ in the SEM : Explanations to the success of DLC coated tools in aluminium forming. Wear 292–293, 49–60.

17. Heinrichs, J., Olsson, M., Jacobson, S.,. 2012, New understanding of the initiation of material transfer and transfer layer build-up inmetal forming—In situ studies in the SEM. Wear 292–293, 61–73.

18. Kirkhorn, L., Bushlya, V., Andersson, M., Stahl, J.-E.,. 2013, The influence of tool steel microstructure on frictionin sheet metal forming. Wear 302, 1268–1278.

19. W. Mocko. 2012, Dynamic Properties of Aluminium Alloys Used in Automotive Industry. *Journal of KONES Powertrain and Transport, Vol. 19, N.2, pp 345-351.*

20. G. Davies. 2003, Materials for Automobile Bodies. Elsevier Ltd. ISBN 0-7506-5692-1.

21. Lazzarotto, L., Dubar, L., Dubois, A., Ravassard, P., Oudin, J.,. 1997, Identification of Coulomb's friction coefficient in real contact conditions applied to a wire drawing process. Wear 211, 54-63.

22. Materials, ASTM E646-00 Standard Test Method for Tensile Strain-Hardening Exponents (n-Values) of Metallic Sheet.

23. Scott, D.W.,. 2011, Sturges' and Scott's Rules. [book auth.] Miodrag Lovrig. *International Encyclopedia of Statistical Science.* ISBN: 3642048978, pp 1563-1566.

24. M. Ruiz-Andrés, A. Conde, J. de Damborenea, I. García,. 2015, Wear behaviour of aluminium alloys at slow sliding speeds. Tribology Transactions , Volume 58, Issue 5.

25. B. N. Pramila Bai & S. K. Biswas. 1986, Effect of Load on Dry Sliding Wear of Aluminum-Silicon Alloys. A S L E Transactions, Volume 29, Issue 1.

26. Spyros I. Tseregounis. 1996, Wear and Galling of 356-T6 Aluminum-on-Steel in Low Amplitude Reciprocating Sliding in the Presence of Synthetic Lubricants in HFC-134a Atmosphere. Tribology Transactions Volume 39, Issue 1.

27. Laurent Dubar, Catalin I. Pruncu, André Dubois, Mirentxu Dubar. 2014, Effects of Contact Pressure, Plastic Strain and Sliding Velocity on Sticking in Cold Forging of Aluminium Billet. Procedia Engineering, Volume 81, Pages 1842-1847.

28. Masters, I.G., Williams, D.K., Roy, R.,. 2013, Friction behaviour in strip draw test of prestretched alluminium alloys. International Journal of Machine Tools & Manufacture 73, 17–24.

Table 1. Class of plastic strains corresponding to different penetration depths

Grade	Ep1	Ep2	Ep3	Ep4	Ep5	No Lubr.
Strain Range	0.006-0.027	0.027-0.048	0.048-0.069	0.069-0.09	0.09-0.112	
Strain mean value	0.014	0.035	0.052	0.073	0.107	0.518

Figure 1. Stress-strain curve of Al6082 aluminum alloy: a) Engineering stress-strain curve; b) True stress-strain curve.

a)

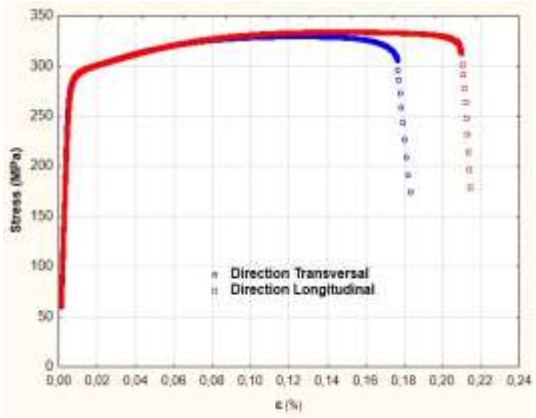

b)

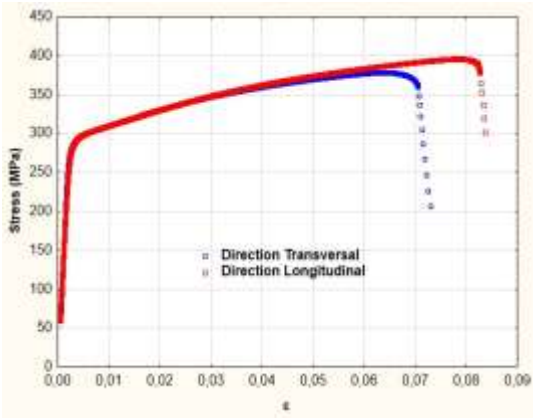

Figure 2. a) Schematic view of the Upsetting-sliding test (UST), and b) Zones of analysis considered for the contactor surface

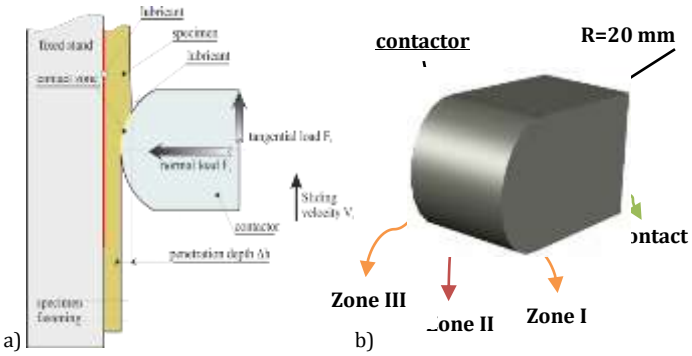

Figure 3. Initial distribution of surface roughness: a) contactor; b) Al6082 specimen

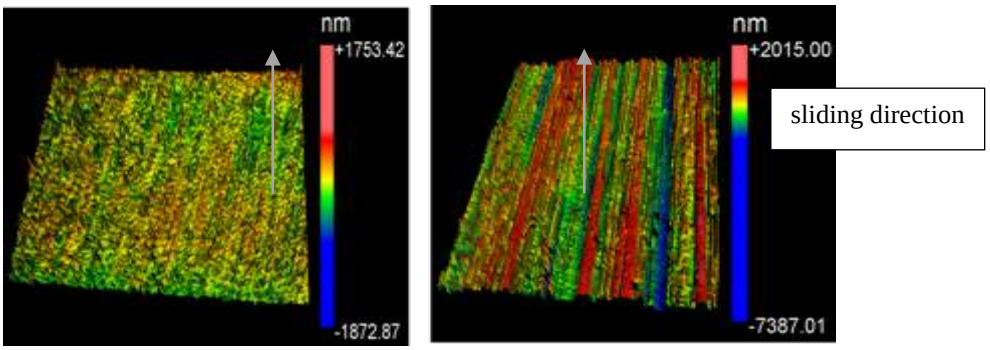

Figure 4. Map of measurement profile a) theoretic curve, b) before test, and c) after test (in zone I, Ep1)

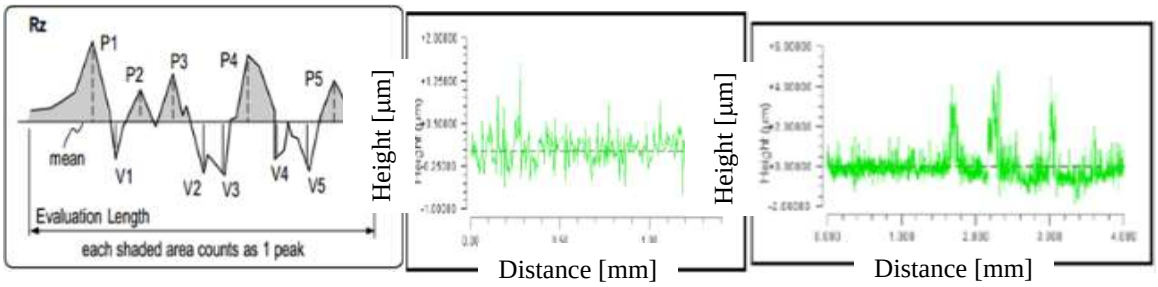

Figure 5. Variation of thickness of the material layer deposited on the tool surface in the UST: a)direction transverse to sliding, and b) longitudinal (i.e. sliding) direction; b)

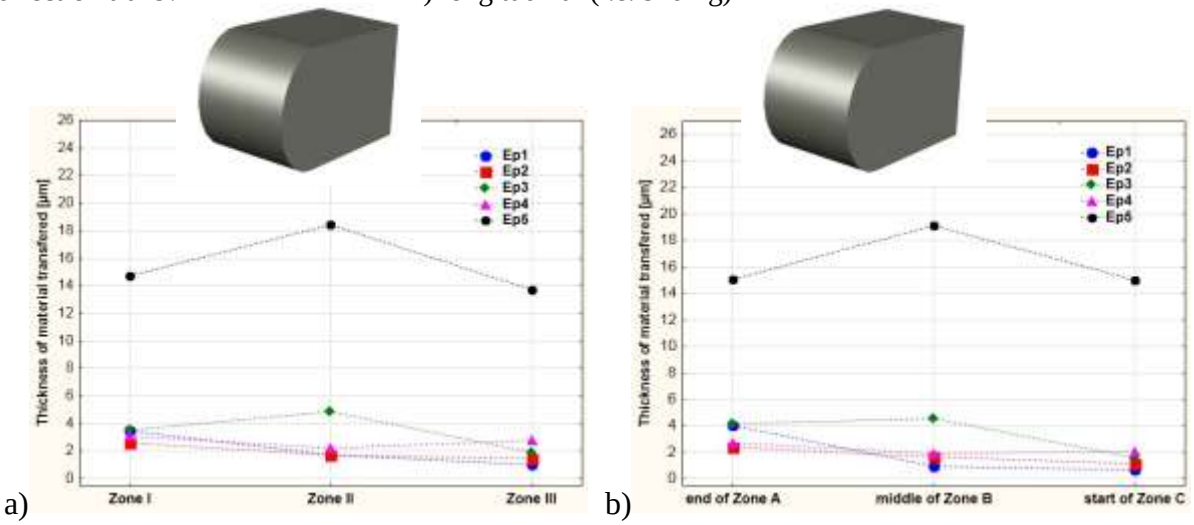

Figure 6. Comparison between 3D-optical profilometry (Figures 6a through 6d) and SEM (Figures 10e through 10h (i.e. red-aluminum transfer, and green-contactor surface), magnification 50X) patterns recorded for the contactor surface (zone I) at different grades of equivalent plastic strain with or without lubrication: Ep1 (a)-(e), Ep4 (b)-(f), Ep5 (c)-(g), No Lub. (d)-(h).

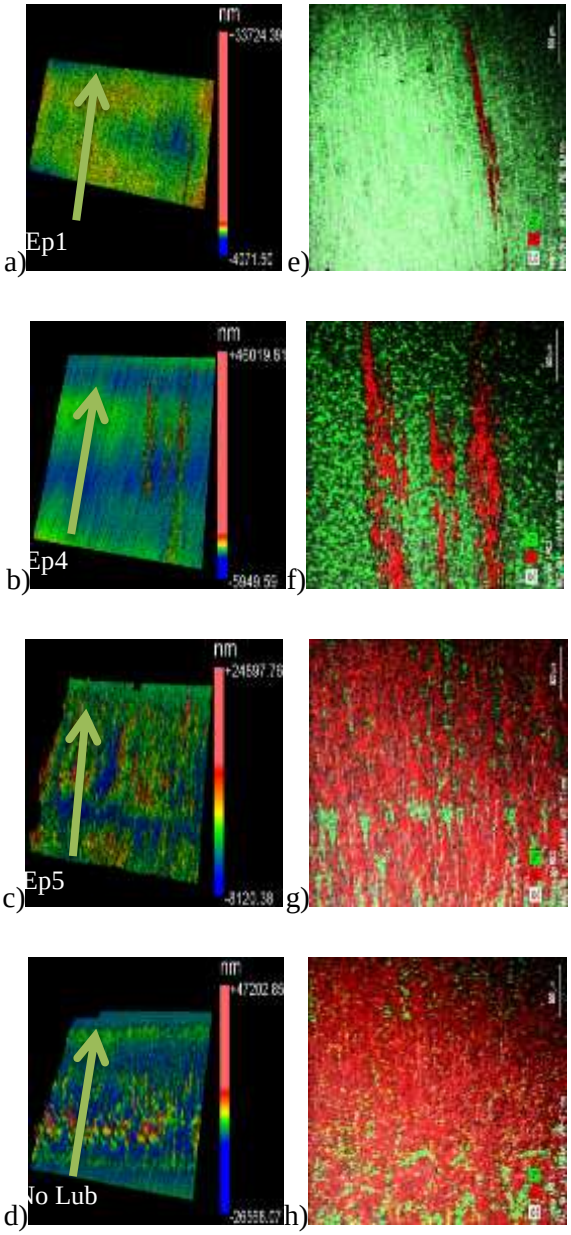

Figure 7. Variation of coefficient of friction as a function of plastic deformation during the UST for different forging speeds

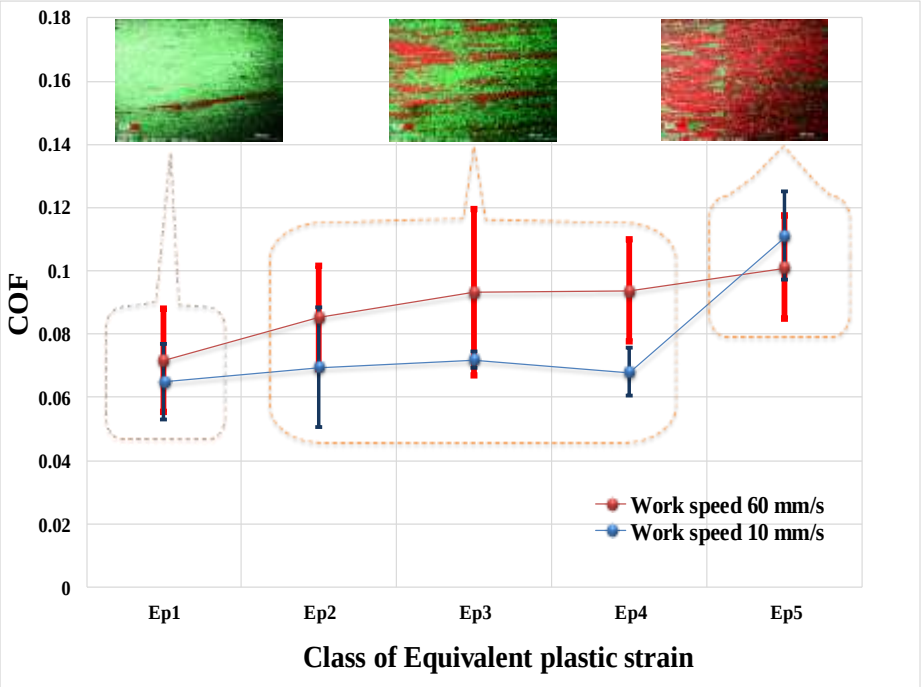

Figure 8. Effect of cold forging of aluminum alloy on the surface integrity

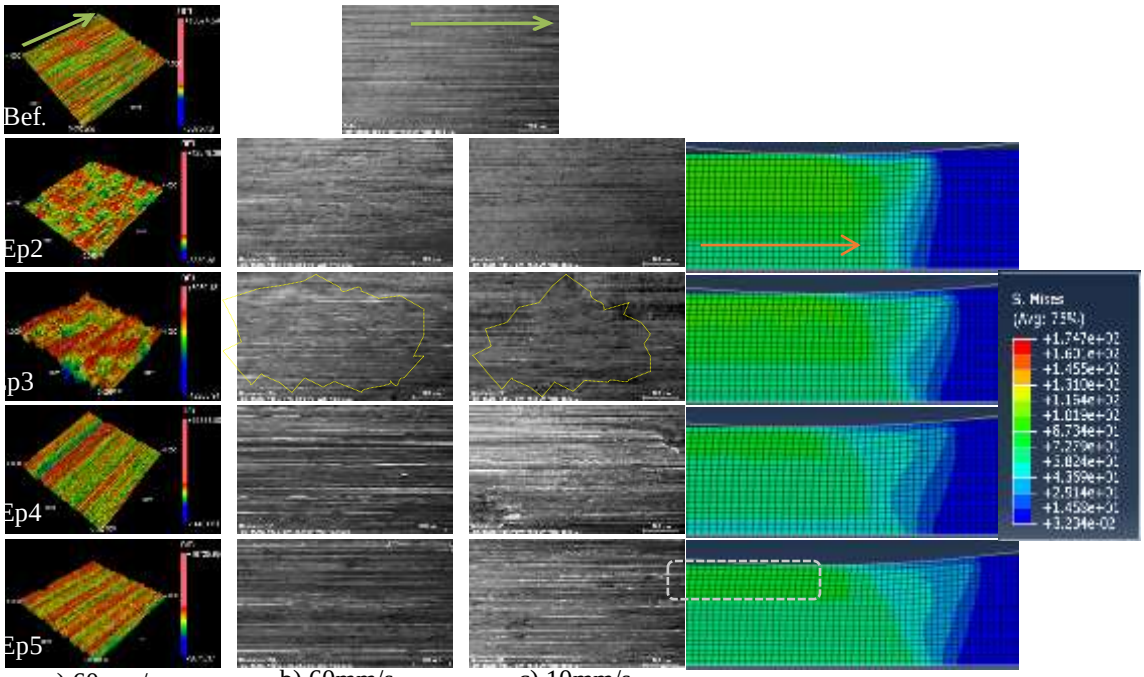

a) 60mm/s b) 60mm/s c) 10mm/s d) 60mm/s

ACCEPTED MANUSCRIPT